Introducing a novel coefficient on mixed-nanoparticles material: relationship between the theoretical and experimental densities

Mansour Ashoor [a], Abdollah Khorshidi [b,*], Leila Sarkhosh [a]

[a] Radiation Application Research School, Nuclear Science and Technology Research Institute, AEOI, Tehran, Iran
[b] School of Paramedical, Gerash University of Medical Sciences, Gerash, Iran

ARTICLE INFO

ABSTRACT

Nanoparticles (NPs) indicating a unique potential in bioradiation and nuclear reactor shielding are employed in many fields due to their particular specifications leading improving the mechanical properties as well as pore structure of the concrete-shield. The aim was to introduce a *novel coefficient* (ξ), namely the experimental to theoretical density ratio for mixed-NPs material at various nanoparticles percent concentrations (ω_{nano}) based on pure mathematical aspects along with the some suitable physical purposes by Monte Carlo method. The change in the mixture density to the change in ω_{nano} is always proportional to the ω_{nano} value. The density will become maximum at the ω_{nano}^{*} in which the physical, morphological and chemical features of NPs along with the amounts of voids in the material have a key role over estimating porosity percentage. The NPs' separation probability as born-cascaded-pairs towards very small radii may be formulated as $\xi - \xi^{-1} + \omega_{nano}^{*} + k^{"}|\omega_{nano} - \omega_{nano}^{*}| = k'$ where k' and $k^{"}$ are constant values. In conclusion, the theoretical results may be experimentally used in future work for different applications such as designing shield at a nuclear facility.

1. Introduction

Nanoparticles (NPs) are able to change some mechanical and physical specifications of materials towards specific purposes, and to improve some parameters such as mass attenuation coefficient at nuclear facilities due to high ratio of surface to volume as well as the optical features [1, 2, 3, 4]. They have also improved the contrast, signal to noise ratio and sensitivity in the images at the various imaging modalities, and their synthesis methods will vary their technical features [5, 6]. The different NPs have been used in concrete mixtures as shield in order to improve both the mechanical properties and pore structure of the concrete [7, 8] which merely change the mixed-material density nonlinearly. This feature is useful to design a shield in nuclear science.

The main purpose of the shields is to protect operating personnel as well as to reduce the effective dose equivalent in all areas in which the occupational dose limit must be consistent with ALARA recommendations. In general, shielding requirements are most important in the design of a nuclear facility. To characterize this matter, the gamma radiation absorption coefficient in some shielding materials such as concrete is measured using point isotropic radioactive sources, which is cumbersome. In contrast, we must calculate and simulate them by Monte Carlo

method in which the amounts of experimental mixed NPs density are needed. As known, the type and density of material affect the amounts of the interactions. Thus, the probability of nuclear radiation absorption is directly proportional with the shield thickness and a coefficient originated from the nanoparticles, which is investigated here. Mesbahi et al. and Tekin et al. [9, 10] have shown that the concrete doped with nanoparticles exhibits a different behavior in high and low energy gamma shielding. Also, Hassan et al. [11] have used nano-PbO and $PbTiO_3$ to study the gamma attenuation coefficient and density. Moreover, Zaghloul et al. [12] used nano-silica with 1%–7% as partially replacement of cement, and their results indicated that 3% nano-silica improves physical, chemical and shielding properties. Here, nano-SiO_2 is added to the normal cement to determine the density.

The aim is to introduce a *novel coefficient* (ξ), namely the experimental to theoretical density ratio for mixed-NPs material at various nanoparticles percent concentrations (ω_{nano}) based on pure mathematical aspects to interpret the attenuation coefficient and density in shielding issues. Elsharkawy's article is chosen for validation of our theory in which the SiO_2 NPs (SONPs) at various concentrations in the cement was investigated by the theoretical-experimental approach to compute the mass attenuation coefficient as a nuclear-shield [2].

---

* Corresponding author.
E-mail address: abkhorshidi@yahoo.com (A. Khorshidi).

2. Theory

This part is an effort to determine a novel coefficient, namely the ratio of experimental density to theoretical one for computation of the experimentally mixed-NPs density. The calculation and simulation by Monte Carlo N-Particle version X (MCNP-X) code using a proper and distinct formula requires the experimental density. Here, the existing experimental density is blended with theoretical density to predict the other densities without any further experimentation. Since there are some chemical reactions after blending, therefore the density will differ. The NPs' separation probability, ξ, as born-cascaded-pairs towards very tiny radii may be obtained as follows:

$$\xi = \cfrac{1}{1+\varepsilon+\cfrac{1}{1+\varepsilon+\cfrac{1}{1+\varepsilon+\cfrac{1}{1+\varepsilon+\cfrac{1}{1+\varepsilon+\cfrac{1}{1+\varepsilon+\cfrac{1}{1+\varepsilon+\cfrac{1}{1+\varepsilon+\cfrac{1}{1+\varepsilon+\cfrac{1}{1+\varepsilon+\dots}}}}}}}}} = \frac{-\varepsilon - 1 + \sqrt{\varepsilon^2 + 2\varepsilon + 5}}{2}$$

(1)

The change in the *mixture density*, ε, to the change in ω_{nano} is always proportional to the ω_{nano} value even in extreme chemical and physical environmental conditions. Therefore, the function of the *mixture density* per ω_{nano} is approximately as parabolic in which the density will become maximum at ω_{nano}^*. The physical, morphological and chemical features of NPs along with the amounts of voids in the material will affect the ω_{nano}^* value. In Eq. (1), one may introduce $\varepsilon = k' + \omega_{nano}^* + k'' |\omega_{nano} - \omega_{nano}^*|$ in which $\omega_{nano}^* = f(R, E, Z, \rho, n)$ where R, E, Z, ρ, and n are the *NPs radius, gamma ray energy, effective atomic number, mass density*, and *electron density*, respectively. The constant values of k', k'' and ω_{nano}^* are obtained by appropriate measurements at different concentrations for each nano-particle. For instance, the ω_{nano}^* value will occur in 1.5 (%) of the concentration of SONPs in the concrete-cement mixture so that $\varepsilon = -0.2 + 0.05 \times |\omega_{nano} - 1.5|$. It is concluded that the increase of SONPs content up to 1.5 (%) increases the total gamma-ray attenuation coefficient for all energies [2].

Here, the MCNP-X code was utilized to simulate the nano-geometry by lattice (LAT) and universe (U) modules. Firstly, the attenuator material and mixed-NPs with the different weight percentages (0.0, 0.5, 1.5, 2.0 and 2.5)% were defined in input file. The process was done by 1E7 primaries. The operation time and the number of histories are dependent on each other. When the code ran by the defined photons or input time, the photons tracked the planned geometry and particle history weights were binned into the energy deposition mesh tally. The track length of the particles (F6 tally) were considered over the mesh score volumes and normalized to be per starting particle.

3. Results

The voids in cement without nanoparticles create a vital role towards decreasing the density as well as the attenuation coefficient. In contrast, they will be gradually filled with increasing nanoparticles so that the density and attenuation coefficient will be increased. In this case, the density value of mixture will be maximized. With more increasing NPs, the density value will be decreased due to the chemical reactions. The chemical analyses of Portland cement are given in Table 1 to verify our theory.

In this study, while the ω_{nano} value is zero, the ε value is considered as -0.125 so that the ξ value will become 0.654. The various values of ξ as a function of the ε ones are indicated in Table 2 derived from Eq. (1).

The experimental, theoretical and modified (our theory) values of densities (g/cm³) for mixed cement with SONPs at different weight percentages (0.0, 0.5, 1.5, 2.0 and 2.5) % along with the relative error values are indicated in Table 3. The minimum and maximum relative errors were 1.41% and 5.75% by 2.5% and 2% of ω_{nano}, correspondingly. Also, Fig. 1 shows the comparison between simulated, calculated and

Table 1
The chemical analyses of Portland cement before doping nano-materials [2].

Elements	Theoretical density (g/cc)	Weight %	Portland Cement
SiO_2	2.648	23.69	0.6273
Al_2O_3	3.97	5.63	0.2235
Fe_2O_3	5.25	3.28	0.1722
CaO	3.34	63.68	2.1269
MgO	3.6	1.38	0.0496
SO_3	1.9	0.19	0.0036
K_2O	2.35	1.18	0.0277
N_2O	0.001799	0.97	0.0017
Total Theoretical Density (ρ^{Theory})	-	100	**3.2325**

theoretical findings of density in terms of weight percentage for mixed cement with SONPs. In simulation, the mean relative error was estimated 0.05 for quality of the scoring evaluation in nano-geometry design. The simulation findings are greater than the experimental ones by a factor of 1.3. From $\omega_{nano} = 0\%$–2.5%, the mixed density showed some fluctuations especially in experiment and simulation results. The density obtained by the proposed method confirmed that the modified-theory values have the closest amounts to the experimental ones. The differences between the maximum and minimum values of mixed density were 0.03, 0.08, 0.17 and 0.12 for theory, modified-theory, experiment and simulation, correspondingly.

4. Discussion

The synthetic method in making NPs plays a key role in acquiring proper properties. Several methods of co-precipitation have been developed along with many bio-molecules and surfactants [13, 14, 15, 16, 17, 18]. Although this method is suitable for NPs synthesis, it has defects such as particle size distribution and the use of a strong base in the reaction process, which may affect the results in the NPs. However, control of particle size, morphology and composition in the pathway of co-precipitation is limited as particle kinetically controlled growth. The size, shape, and composition of NPs are based on many factors, such as the pH of reaction system and the ionic strength of the medium [19], in which case these intrinsically affect the defined coefficients that their examinations in detail are beyond the scope of our research. Ordinarily, different techniques are employed for preparation of nanoparticles such as chemical vapor deposition, synthesis by plasma, micro emulsion procedures, combustion synthesis, sol-gel projecting, hydrothermal methods and so on. The optimized particle size in mixture density is typically controlled by pH adjustment and temperature variations. By increasing the reaction temperature there is more energy within the mixture, this would increase mobility and cause a greater number of collisions between the particles [20, 21]. The relation between NPs size and peak widening is defined by Bragg diffraction angle of XRD (X-ray powder diffraction) patterns and the X-ray wavelength. Meanwhile, the scanning electron microscopy (SEM) is utilized for morphology descriptions of NPs. The thermo-gravimetric analysis (TGA) is used to estimate the thermal characteristics and mass loss, and the infrared spectroscopy (IR) is performed for interaction and complex type determination and combination (bonding) blueprint by wave number separation.

Here, there are several obvious factors affecting the protection needed in the facility. As it is known, the use of concrete in nuclear facilities is designed to contain and protect from radiation and radioactive materials as well as to depose spent nuclear fuel which its characteristic is essential for the safe operation of the facility [22]. Therefore, as a good protective material, concrete has a proper structural strength [23], which is considered to be the main material in which NPs are dispersed. The SONPs are in agglomerated dry powder or colloidal shapes that work significantly dissimilar in cement. The Ca–Si-hydrate is mostly shaped during the cement paste hydration as a foremost constituent besides Ca hydroxide that leaches out throughout hydration.

Table 2

The various values of ξ as a function of the ε ones.

ε	-0.300	-0.275	-0.250	-0.225	**-0.200**	-0.175	**-0.150**	**-0.125**	-0.100	-0.075	-0.050	-0.025	0
ξ	0.7095	0.7012	0.693	0.685	**0.677**	0.6692	**0.6616**	**0.654**	0.6466	0.6393	0.6321	0.625	0.618

Three bold amounts are considered for Table 3.

Table 3

The experimental, theoretical and modified values of densities (g/cm^3) mixed cement with SONPs at different weight percentages along with the relative error values, (ε = -0.25 → ξ = 0.693) [2].

ω_{nano} (%)	ε	ξ	ρ^{Theory}	$\rho^{Experimental}$	$\rho^{Modified-Theory}$	Relative error % ($\rho^{E.}$- $\rho^{T.}$)	Relative error % ($\rho^{E.}$- $\rho^{M.T.}$)
0.0	-0.12	0.654	3.23	2.15	2.11	50.23	1.86
0.5	-0.15	0.661	3.22	2.17	2.13	48.39	1.84
1.5	-0.20	0.677	3.21	2.30	2.18	39.56	5.22
2.0	-0.15	0.661	3.21	2.26	2.13	42.03	5.75
2.5	-0.12	0.654	3.20	2.13	2.10	50.23	1.41

NPs in concrete mix are used to improve mechanical properties and structure of concrete pores cooperatively [24, 25]. The effect of these particles, mostly SONPs, has been inspected by many researchers. Tao [26] examined the permeability of the water and concrete structure in micro-size containing the SONPs and reported that the presence of SONPs could improve the resistance to water penetration in concrete samples. In addition, Bashter et al. [27] demonstrated that the microstructure of concrete containing SONPs was more compressed, and these particles improved the structure of concrete pores. Several studies have shown that pozzolanic activity of SONPs is more than silica fume and its positive effects on the mechanical properties of hardened cement [28, 29]. Researchers further claim that the amount of crystals in hydrated cement increases as a result of increasing NPs values [30]. The NPs fill the cement pores, so its strength increases. Increasing SONPs' amounts by more than 1.5% reduces the compressive strength, this behavior is related to the accumulation of SiO2 particles, which shows more voids in concrete and reduces C$_3$S content [31]. The effect of SONPs on the compressive strength of concrete and the relationship between the density percentage and content of SONPs by weight were performed by Elsharkawy et al. [2]. Their results indicate that the density increases by 1.5% as SONPs increase, because NPs fill cavity holes, so the density of concrete increases, but for concrete samples 2 and 2.5%, the density of concrete decreases. When SONPs content increases by more than 1.5%, SONPs' inference with each other increases so that the internal voids increases in the concrete mixture, which leads to a reduction in total density [32]. Changes in the *mixture density* to changes in SNOPs are proportional to the SONPs value at any situation. Hence, the function of the *mixture density* per SONPs percent concentrations is nearly as parabolic in which the density will be converted to a maximum at any special

concentration. SONPs in concrete mixture improve the structure of concrete pores due to the performance of SONPs as nano filler rather than the formation of more hydrated products. The results of this study showed that the addition of SONPs improves the mechanical and nuclear properties of concrete. When a small amount of NPs are dispersed uniformly in the cement paste, the NPs are strongly bound to cement hydrates as a nucleus and, due to their high activity, reinforce hydration cement, which is suitable for cement resistance. In addition to that, the NPs among the hydrate products prevent the growth of crystals that are not suitable for cement resistance. The SONPs can help in the hydration process to produce more C–S–H by way of Ca(OH)$_2$ reaction [31].

In general, the linear attenuation coefficient is the simplest absorption coefficient to measure experimentally, but it is not usually tabulated because of its dependence on the density of the absorbing material. Since the gamma rays mainly interact with atomic electrons, the attenuation coefficient and the electron density are proportional. On the other hand, the electron density depends on the bulk density of the absorbent substance and their ratio is constant, atomic number to atomic mass, regardless of bulk density. This ratio is nearly constant for all except the heaviest elements and hydrogen [33, 34, 35, 36]. This dependence for nanoparticles is very complex. There are deviations between theoretical and experimental values of both linear and mass attenuation coefficients. These deviations may be characterized with introducing the ξ parameter by Eq. (1).

As it was said, a gamma ray may interact with an atom in a bound state, in which the electron loses its entire energy and ceases to exist as a gamma ray [37, 38, 39, 40]. Two phenomena of Compton incoherent scattering and photoelectric effect are the most important mechanism of interaction in nuclear domains when gamma radiation energy is low. When sources are used with multiple energies, the evaluation of the attenuation coefficients becomes more complicated. These coefficients are function of electron density, mass density, effective energy, and effective atomic number. Again, this dependence on nanoparticles is very complex. Since the effective energy for different materials of the same thickness is different, it introduces the error. The error is a powerful function of energy associated with the energy spectrum [41]. The difference in the coefficients of attenuation is mainly due to two factors: the effective atomic number of the material in the low-energy range, which is effective at about one quarter of the atomic number power, and the effect of the electron density at high energy (more than 50 keV), which is mainly in the Compton interaction range. Both theoretical and experimental results severely affirm the concept of modulation of the atomic number in the low energy range, while the modulation-dependent electron density at higher energies is dominant. In addition, the mass attenuation coefficient decreases with increasing energy of γ-ray. In general, this reducing is largely the result of Compton scattering and some photoelectric interactions [42, 43, 44, 45, 46].

The highest amount of linear and mass attenuation coefficients was found at the lowest energy of 0.511 MeV, but the lowest value was
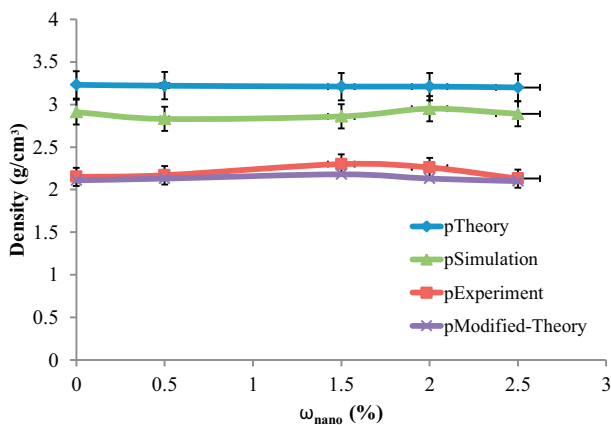

Fig. 1. Density of mixed cement with SONPs versus diverse weight percentages in Theory, Modified-Theory, Experiment and Simulation.

found at the highest energy of 1.33 MeV. The probability of radiation absorption of the nucleus is directly proportional to the thickness of the shield and the geometric coefficient of the nanoparticles.

Mesbahi et al. [9] have shown that the concrete doped with nanoparticles have a greater neutron removal cross section than microparticles, but in high energy gamma shielding had less effetcs. Also, Tekin et al. [10] demonstrated the increasing of mass attenuation coefficient via doping of nano-$BaSO_4$ into lead by %1.4609 ratio for 0.500 MeV of gamma source and it led to more radiation absorbtion. Furthermore, Hassan et al. [11] have investigated the particle size on concrete attenuation and density by doping PbO and $PbTiO_3$ nano powders via co-precipitation and oxalate precursor methods, so that the defect density decreased by increasing nano-PbO contents and also the gamma attenuation coefficient improved. They have reported 2.290 and 2.410 g/cm^3 density by adding %30 nano-PbO and $PbTiO_3$, respectively. In this study by adding %1.5 nano-SiO_2 to normal cement, the $\rho^{\text{Modified-Theory}}$ reached a maximum of 2.18 ± 0.05 g/cm^3.

Some systems are used to monitor the radiation shielding efficiency [47, 48] or to measure the fast neutrons besides gamma rays [49, 50, 51, 52, 53, 54, 55, 56]. In such systems, the use of nanomaterials against radiation would be preferable. Akkurt et al. [57] have demonstrated that the linear attenuation coefficient for all types of concretes is a function of the concrete's density. Since the different concretes have different densities, Bento et al. [58] have shown that the mass attenuation coefficient for a fibrous self-compacting concrete is higher than those for ordinary concrete of about 5% depending on the gamma energy, and the density is higher than ordinary concrete, 2.4 and 1.9 g/cm^3 correspondingly. Meanwhile, Qafleshi et al. [59] have compared the percentage of fly ash in concrete mixtures and demonstrated that the activity concentrations of ^{40}K, ^{226}Ra and ^{232}Th are very low in all concrete specimens varied from 0.046 to 0.054 mSv per year.

With the increasing use of radioactive isotopes and accelerators in various applications, such as medicine, industry, and power generation, it is also becoming increasingly necessary to reduce the dose to the employees and the public. The equipments that deal with ionizing radiation of any kind must comply with the safety necessities, and at this time the shielding estimations come into play. The thick concrete in walls, floor and ceiling requires a plenty of space, particularly in the cases of adaptations of an existing building or a space for the first handling, which causes an enormous restriction in utilizable space for the device. The normal concrete is a comparatively low-cost material than the lead, which requires larger thickness for the identical shielding effect by virtue of its relatively lower attenuation coefficient.

5. Conclusion

The most important material for shielding is concrete in nuclear facilities which the performace can be improved by addition some NPs at the various concentrations. In this study, we could estimate the experimentally mixed-NPs material density using the theoretical density along with the defined coefficient. The minimum relative error was found 1.41% by 2.5% of ω_{nano}. Here, the theoretical and existing experimental densities were mixed to forecast the other densities as a byway without any experimental effort. Also, MCNP simulations by variance reduction techniques were employed to reduce the relative error of a scoring tool or its variance for a fixed computing time. The mean relative error was estimated 0.05 for quality of the scoring evaluation in simulated nano-geometry plan. For future work, the proposed coefficient will use to simulate the mixed-NPs by FLUKA or GEANT4 in which the simulation and experiment densities are not determined simultaneously.

Declarations

Author contribution statement

Abdollah Khorshidi: Conceived and designed the experiments;

Performed the experiments; Analyzed and interpreted the data; Contributed reagents, materials, analysis tools or data; Wrote the paper.

Mansour Ashoor: Conceived and designed the experiments; Performed the experiments; Analyzed and interpreted the data.

Leila Sarkhosh: Analyzed and interpreted the data.

Competing interest statement

The authors declare no conflict of interest.

Additional information

No additional information is available for this paper.

References

[1] H. Aleali, L. Sarkhosh, R. Karimzadeh, N. Mansour, Threshold-tunable optical limiters of Au nanoparticles in castor oil, J. Nonlinear Opt. Phys. Mater. 21 (2) (2012) 1250024.

[2] E.R. Elsharkawy, M.M. Sadawy, Effect of gamma ray energies and addition of nano-SiO$_2$ to cement on mechanical properties and mass attenuation coefficient, IOSR J. Mech. Civ. Eng. 13 (6) (2016) 17–22.

[3] L. Sarkhosh, N. Mansour, Study of the solution thermal conductivity effect on nonlinear refraction of colloidal gold nanoparticles, Laser Phys. 25 (6) (2015), 065404.

[4] L. Sarkhosh, H. Aleali, R. Karimzadeh, N. Mansour, Large thermally induced nonlinear refraction of gold nanoparticles stabilized by cyclohexanone, Phys. Status Solidi 207 (10) (2010) 2303–2310.

[5] G. Gao, X. Liu, R. Shi, K. Zhou, Y. Shi, R. Ma, E. Takayama-Muromachi, G. Qiu, Shape-controlled synthesis and magnetic properties of monodisperse Fe$_3$O$_4$ nanocubes, Cryst. Growth 10 (7) (2010) 2888–2894.

[6] A. Khorramdoust, M. Ashoor, K. Saberyan, A. Eidi, Synthesis and characterization of magnetite nanoparticles coated with folic acid as targeted MRI contrast agents, Dig. J. Nanomater. Biostruct. 12 (3) (2017) 909–915.

[7] M.T. Madsen, J.A. Anderson, J.R. Halama, J. Kleck, D.J. Simpkin, J.R. Votaw, R.E. Wendt, L.E. Williams, M.V. Yester, AAPM task group 108: PET and PET/CT shielding requirements, Med. Phys. 33 (2006) 4–15.

[8] H.O. Tekin, MCNP-X Monte Carlo code application for mass attenuation coefficients of concrete at different energies by modeling 3 × 3 inch NaI(Tl) detector and comparison with XCOM and Monte Carlo data, Sci. Technol. Nucl. Ins. 2016 (2016) 1–7.

[9] A. Mesbahi, H. Ghiasi, Shielding properties of the ordinary concrete loaded with micro- and nano-particles against neutron and gamma radiations, Appl. Radiat. Isot. 136 (2018) 27–31.

[10] H.O. Tekin, V.P. Singh, U. Kara, T. Manici, E.E. Altunsoy, Investigation of nanoparticle effect on radiation shielding property using Monte Carlo method, CBU. J. of Sci. 12 (2) (2016) 195–199.

[11] H.E. Hassan, H.M. Badran, A. Aydarous, T. Sharshar, Studying the effect of nano lead compounds additives on the concrete shielding properties for γ-rays, Nucl. Instrum. Methods B 360 (2015) 81–89.

[12] Y.R. Zaghloul, S.K. Elwan, Characterization of nano-silica concrete for nuclear uses, Int. J. Curr. Eng. Technol. 7 (1) (2017) 207–212.

[13] M. Mahdavi, M. Bin Ahmad, M.J. Haron, F. Namvar, B. Nadi, M.Z. Rahman, J. Amin, Synthesis, Surface modification and characterisation of biocompatible magnetic iron oxide nanoparticles for biomedical applications, Molecules 18 (7) (2013) 7533–7548.

[14] H. Heinz, C. Pramanik, O. Heinz, Y. Ding, R.K. Mishra, D. Marchon, R.J. Flatt, I. Estrela-Lopis, J. Llop, S. Moya, R.F. Ziolo, Nanoparticle decoration with surfactants: molecular interactions, assembly, and applications, Surf. Sci. Rep. 72 (1) (2017) 1–58.

[15] A. Ali, H. Zafar, M. Zia, I. Haq, A.R. Phull, J.S. Ali, A. Hussain, Synthesis, characterization, applications, and challenges of iron oxide nanoparticles, Nanotechnol. Sci. Appl. 9 (2016) 49–67.

[16] A. Ruíz-Baltazar, R. Esparza, G. Rosas, R. Pérez, Effect of the surfactant on the growth and oxidation of iron nanoparticles, J. Nanomater. 240948 (2015) 1–8.

[17] Y. Bahari Molla Mahaleh, S.K. Sadrnezhaad, D. Hosseini, NiO nanoparticles synthesis by chemical precipitation and effect of applied surfactant on distribution of particle size, J. Nanomater. 470595 (2008) 1–4.

[18] A. Khorshidi, M. Ahmadinejad, S.H. Hosseini, Evaluation of a proposed biodegradable ^{188}Re source for brachytherapy application: a review of dosimetric parameters, Medicine (Baltim.) 94 (28) (2015) e1098.

[19] S. Wu, A.Z. Sun, F.Q. Zhai, J. Wang, W.H. Xu, Q. Zhang, A.A. Volinsky, Fe$_3$O$_4$ magnetic nanoparticles synthesis from tailings by ultrasonic chemical co-precipitation, Mater. Lett. 65 (12) (2011) 1882–1884.

[20] Y.P. Singh, A. Abhishek, S.J. Pawar, Characterization of silica nano-particles synthesized by thermo-mechanical, Int. J. Adv. Res. Sci. Eng. 6 (5) (2017) 267–272.

[21] L.P. Singh, S.K. Agarwal, S.K. Bhattacharyya, U. Sharma, S. Ahalawat, Preparation of silica nanoparticles and its beneficial role in cementitious materials, Nanomater. Nanotechnol. 1 (1) (2011) 44–51.

[22] R.S. Chen, Q. Ye, Research on the comparison of properties of hardend cement paste between Nano-SiO$_2$ and silicafume added, Concrete J. 1 (1) (2002) 7–10.

[23] Q. Ye, Research on the comparison of pozzolanic activity between Nano-SiO$_2$ and silica fume, Concrete J. 1 (3) (2001) 19–22.

[24] L. Raki, J. Beaudoin, R. Alizadeh, J. Makar, T. Sato, Cement and concrete nanoscience and nanotechnology, Materials (Basel) 3 (2010) 918–942.

[25] F. Pacheco-Torgal, S. Miraldo, Y. Ding, J.A. Labrincha, Targeting HPC with the help of nanoparticles: an overview, Constr. Build. Mater. 38 (2013) 365–370.

[26] J. Tao, Preliminary study on the water permeability and microstructure of concrete incorporating Nano-SiO$_2$, Cement Concr. Res. 10 (35) (2012) 1943–1947.

[27] I.I. Bashter, A. El-Sayed Abdo, A.S. Makarious, A comparative study of the attenuation of reactor thermal neutrons in different types of concrete, Ann. Nucl. Energy 23 (14) (1996) 1189–1195.

[28] I.I. Bashter, Effect of silica fume addition to concrete mixes on Radiation Attenuation Properties, Arab. J. Nucl. Sci. Appl. 34 (2001) 179–189.

[29] A. Khorshidi, J. Soltani-Nabipour, F. Sadeghi, Constructing environmental radon gas detector and measuring concentration in residential buildings, Phys. Part. Nucl. Lett. 16 (6) (2019). In press.

[30] A. Saetta, R. Vitaliani, Experimental investigation and numerical modeling of carbonation process in reinforced concrete structures Part I: theoretical formulation, Cement Concr. Res. 34 (2004) 571–579.

[31] S. Gopinath, P.C. Mouli, A.R. Murthy, N.R. Iyer, S. Maheswaran, Effect of nano silica on mechanical properties and durability of normal strength concrete, Arch. Civ. Eng. 4 (2012) 433–444.

[32] A.A. Abd El-Latif Ahmed, K.S. Saeid, H.S. Ragab, A.A. Abdalla, Effect of gamma ray energies and addition of iron slag by weight to Portland cements on mass attenuation coefficient, J. Mater. Sci. Eng. A 3 (12) (2013) 838–842.

[33] G. Nelson, D. Reilly, Gamma-ray interactions with matter, in: Passive Non-destructive Analysis of Nuclear Materials, Los Alamos National Laboratory, 1991, pp. 90–732. NUREG/CR-5550, LAUR.

[34] Y. Ichikawa, G. England, Prediction of moisture migration and pore pressure build-up in concrete at high temperatures, Nucl. Eng. Des. 228 (1-3) (2004) 245–259.

[35] A. Khorshidi, A. Rajaee, M. Ahmadinejad, M. Ghoranneviss, M. Ettelaee, Low energy electron generator design and depth dose prediction for micro-superficies tumor treatment purposes, Phys. Scripta 89 (9) (2014) 095001–095006.

[36] M. Ashoor, A. Khorshidi, L. Sarkhosh, Estimation of microvascular capillary physical parameters using MRI assuming a pseudo liquid drop as model of fluid exchange on the cellular level, Rep. Practical Oncol. Radiother. 24 (1) (2019) 3–11.

[37] Z.C. Kan, K.C. Pei, C.L. Chang, Strength and fracture toughness of heavy concrete with various iron aggregate inclusions, Nucl. Eng. Des. 228 (2004) 119–127.

[38] A. Khorshidi, Exploration of adiabatic resonance crossing through neutron activator design for thermal and epithermal neutron formation in [99]Mo production and BNCT applications, Cancer Biother. Radiopharm. 30 (2015) 317–329.

[39] A. Khorshidi, Gold nanoparticles production using reactor and cyclotron based methods in assessment of [196,198]Au production yields by [197]Au neutron absorption for therapeutic purposes, Mater. Sci. Eng. C 68 (2016) 449–454.

[40] A. Khorshidi, Accelerator driven neutron source design via beryllium target and [208]Pb moderator for boron neutron capture therapy in alternative treatment strategy by Monte Carlo method, J. Cancer Res. Ther. 13 (3) (2017) 456–465.

[41] Z.H. Cho, J.P. Jones, M. Singh, Foundations of Medical Imaging, John Wiley & Sons Inc, New York, 1993.

[42] M. Ashoor, A. Asgari, A. Khorshidi, A. Rezaei, Evaluation of Compton attenuation and photoelectric absorption coefficients by convolution of scattering and primary functions and counts ratio on energy spectra, Indian J. Nucl. Med. 30 (3) (2015) 239–247.

[43] A. Asgari, M. Ashoor, L. Sarkhosh, A. Khorshidi, P. Shokrani, Determination of gamma camera's calibration factors for quantitation of diagnostic radionuclides in simultaneous scattering and attenuation correction, Curr. Radiopharm. 12 (1) (2019) 29–39.

[44] A. Khorshidi, M. Ashoor, S.H. Hosseini, A. Rajaee, Estimation of fan beam and parallel beam parameters in a wire mesh design, J. Nucl. Med. Technol. 40 (2012) 37–43.

[45] A. Khorshidi, M. Ashoor, S.H. Hosseini, A. Rajaee, Evaluation of collimators' response: round and hexagonal holes in parallel and fan beam, Prog. Biophys. Mol. Biol. 109 (2012) 59–66.

[46] A. Khorshidi, M. Ashoor, Modulation transfer function assessment in parallel beam and fan beam collimators with square and cylindrical holes, Ann. Nucl. Med. 28 (2014) 363–370.

[47] A.M. Gribushin, A.I. Demianov, A.A. Ershov, A.A. Kaminskiy, V.S. Lukanin, V.A. Pikalov, A neutron field monitoring system for collider experiments, Instrum. Exp. Tech. 60 (2) (2017) 167–174.

[48] J.S. Nabipour, A. Khorshidi, Spectroscopy and optimizing semiconductor detector data under X and γ photons using image processing technique, J. Med. Imaging Radiat. Oncol. 49 (2) (2018) 194–200.

[49] A. Khorshidi, Accelerator-based methods in radio-material [99]Mo/^{99m}Tc production alternatives by Monte Carlo method: the scientific-expedient considerations in nuclear medicine, J. Multiscale Model. 10 (1) (2019) 1930001.

[50] N.A. Uvarov, A.V. Galkin, A.V. Grigorenko, V.M. Gorbachev, F.G. Shalata, V.L. Maiornikova, V.S. Maiornikov, V.E. Ablesimov, V.V. Glushikhin, Y.N. Pepelyshev, A.F. Rogov, Measuring the pulse form of neutrons from the ИБР-2 periodically pulsed reactor over a wide pulse-power range, Instrum. Exp. Tech. 46 (2) (2003) 143–148.

[51] N.K. Abrosimov, L.A. Vaishnene, A.S. Vorob'ev, E.M. Ivanov, G.F. Mikheev, G.A. Ryabov, M.G. Tverskoi, O.A. Shcherbakov, Development and experimental study of the neutron beam at the synchrocyclotron of the Petersburg Nuclear Physics Institute for radiation tests of electronic components, Instrum. Exp. Tech. 53 (4) (2010) 469–476.

[52] M. Ashoor, A. Khorshidi, Evaluation of crystals' morphology on detection efficiency using modern classification criterion and Monte Carlo method in nuclear medicine, Proc. Natl. Acad. Sci., India, Sect. A Phys. Sci. (2018). In press.

[53] A. Khorshidi, Neutron activator design for [99]Mo production yield estimation via lead and water moderators in transmutation's analysis, Instrum. Exp. Tech. 61 (2) (2018) 199–204.

[54] A. Khorshidi, A. Pazirandeh, Molybdenum transmutation via [98]Mo samples using bismuth/lead neutron moderators, Europhys. Lett. 123 (2018) 12001.

[55] A. Khorshidi, J.S. Nabipour, Report on correlation between Radon outgassing and aftershocks activity along the bam fault in Kerman province of Iran, Braz. J. Rad. Sci. 5 (2017) 1–12.

[56] A. Khorshidi, Molybdenum-99 production via lead and bismuth moderators and milli-structure-[98]Mo samples by indirect production technique using Monte Carlo method, Phys. Usp. (2018).

[57] I. Akkurt, C. Basyigit, S. Kilincarslan, B. Mavi, A. Akkurt, Radiation shielding of concretes containing different aggregates, Cement Concr. Compos. 28 (2) (2006) 153–157.

[58] W.V. Bento, L.A.M. Magalhães, C.C. Conti, Attenuation coefficients for fibrous self-compacting concrete in the energy range of 50-3000keV, Braz. J. Rad. Sci. 5 (1) (2017) 1–10.

[59] M. Qafleshi, M. Misini, D.R. Kryeziu, L. Aliko, The characterization of naturally occurring radionuclides in concrete incorporating fly ash as partial cement replacement, Braz. J. Rad. Sci. 6 (1) (2018) 1–11.